Macromolecular Materials and Engineering
www.mme-journal.de

Fluorine-Free Superhydrophobic Coatings: Rapid Fabrication and Highly Efficient Oil/Water Separation

*Ítalo G. M. da Silva, Elizabete F. Lucas, and Rigoberto Advincula**

In this work, a rapid method is demonstrated to obtain a fluorine-free superhydrophobic/superoleophilic coating by a simple two-step method: dip-coating and oven curing. The chemical structure of the coating is based on the crosslinking reaction of an alkyl methacrylate, a dimethacrylate (crosslinker) and a silane (adhesive), using AIBN as initiator, toluene as solvent, and silica nanoparticles to enhance surface roughness. Chemorheology results show that the coating is fully cured even in 20 min at 100 °C, exhibiting a water contact angle (CA) of 162 ± 2°, sliding angle (SA) of 4 ± 1°, nanometrical structures throughout the surface, and excellent adhesion properties for the mesh screen. The coating exhibits outstanding oil/water separation efficiency (96–99%) for seven different types of oil (gasoline, diesel, petroleum ether, hexane, toluene, chloroform, and dichloromethane), and in addition presents high recyclability. Based on nonisothermal TGA, the activation energy of degradation, calculated using the Kissinger and Ozawa models, is 113.5 and 114 kJ mol^{-1}, respectively. Finally, the coating is thermally aged at 150 °C: the CA exhibits a smooth decrease up to 129 ± 1° at 120 min, and FTIR analysis shows structural changes possibly related to the generation of thermal oxidation products.

1. Introduction

Despite the significant growth on the use of renewable energies over the past decade, oil has been the leading source of energy in the globe for many decades, and it is estimated to remain on top by 2040.[1] In 2019, about 3.39 billion barrels of gasoline were consumed in the United States, averaging 9.28 million barrels per day.[2] The extensive amount of petrochemicals used in our daily life goes much beyond transportation, as they are also used in many chemical industries for a number of applications, from plastics to asphalt.[3–5] During drilling and production operations, as well as during the transportation of petroleum and its derivatives, different factors can lead to the occurrence of catastrophic spills, such as mishandling, leakage, explosion and other accidents. Regardless of the cause, oil spills can have enormous environmental, economic and social effects. In 2010, the deepwater horizon blowout in the Gulf of Mexico resulted in 11 deaths, released hundreds of tons of oil in the ocean, and costed billions of dollars in fines and remediation.[6–8]

Traditionally, oil/water separation methods include gravity separation, air flotation, filtration, centrifugation, and the use of chemical absorbent materials. However, these methods are generally slow, expensive, and can have a low separation efficiency. Skimming and burning are even less attractive methods, since they have a poorer performance and further harm the environment, respectively.[9,10] Therefore, the development of highly efficient, fast, cost-effective and environmentally friendly technologies to separate oil/water mixtures remains a challenge.

Superhydrophobic coatings have gained a lot of attention in the past years, and they have been used as anticorrosion, self-cleaning, antifog, and anti-ice surfaces. Moreover, inspired by the non-wetting property of the lotus leaf, superhydrophobic coatings have been deposited on mesh screens as a strategy for oil/water separation.[9–14] By definition, a surface is considered superhydrophobic when the water contact angle (CA) is greater than 150°, and the sliding angle (SA) is less than 10°. On the other hand, for a superoleophilic surface, the contact angle between an oil droplet and the surface is less than 10°. Taking advantage of a porous substrate like a mesh screen, the superhydrophobic/superoleophilic coated surfaces not only repel the water molecules, but selectively absorbs the oil, allowing its separation from the mixture by letting it flow through the pores.[14–16]

Many superhydrophobic coatings have been developed based on fluoroalkyl molecules.[16–19] However, per- and polyfluoroalkyl substances (PFAS) can accumulate in the human and

Í. G. M. da Silva, Prof. R. Advincula
Case Western Reserve University
Department of Macromolecular Science and Engineering
Cleveland, OH 44106, USA
E-mail: rca41@case.edu
Í. G. M. da Silva
Universidade Federal do Rio de Janeiro
Escola de Química
Rio de Janeiro 21941-909, Brazil
Prof. E. F. Lucas
Universidade Federal do Rio de Janeiro
Instituto de Macromoléculas
Rio de Janeiro 21941-598, Brazil
Prof. R. Advincula
University of Tennessee
Knoxville, TN 37996 and Oak Ridge National Laboratory
1 Bethel Valley Rd., Oak Ridge, TN 37830, USA
The ORCID identification number(s) for the author(s) of this article can be found under https://doi.org/10.1002/mame.202000400.

DOI: 10.1002/mame.202000400

animal bodies by ingestion (when eating food or drinking liquids contaminated with PFAS), generating very severe health effects, such as thyroid hormone disruption and cancer. The U.S. Environmental Protection Agency (EPA) made an action plan to protect public health from the PFAS effects. As a result, perfluorooctanoic acid (PFOA) and perfluorooctane sulfonate (PFOS) are no longer produced in the United States.[20,21] Besides the serious health consequences of bioaccumulation, these substances are also considered persistent in the environment, as they can pollute ground water and aquatic wildlife.[11]

Efforts have been made to obtain fluorine-free superhydrophobic coatings for oil/water separation. Zhang and co-workers developed a superhydrophobic/superoleophilic coating based on epoxy resin and SiO_2 nanoparticles, and evaluated the oil/water separation with five different types of oil (chloroform, diesel, hexane, kerosene, and toluene), where the efficiency of separation ranged from ≈93 to 97.5%. The mechanical integrity of the coating was assessed through simple sandpaper abrasion and scratch tests.[13] In a similar approach, Cao and co-workers described a polyurethane-based superhydrophobic/superoleophilic coating, and the separation efficiency of mixtures of water and five oils (hexane, kerosene, petroleum ether, tetrachloromethane and toluene) was higher than 94%. The authors performed a peeling test with a sellotape to evaluate the mechanical durability of the coating.[9] Particularly, the Advincula group has reported multifunctional fluorine-free superhydrophobic coatings based on different chemistries, including rubber-modified polybenzoxazine,[12] poly(N-isopropylacrylamide),[22] polystyrene/multiwalled carbon nanotubes,[23] and electrodeposited polythiopenes.[4,24–27]

Herein, we present how to rapidly obtain a fluorine-free superhydrophobic/superoleophilic coating based on common methacrylate chemistry, in a simple and efficient two-step procedure. The oil/water separation efficiency was evaluated for seven oils of commercial interest (gasoline, diesel, petroleum ether, hexane, toluene, chloroform, and dichloromethane). Also, isothermal and nonisothermal thermogravimetry (TGA) were performed, and the degradation profiles were described by thermokinetic models. Finally, the coatings were submitted to thermal ageing, and the wettability and structural changes were discussed with CA and FTIR data, respectively. While other papers often focus on the mechanical integrity of the superhydrophobic coatings upon physical stresses,[9,13,14,19,28,29] there is still very few reports on their thermal behavior, stability, and degradation.

2. Experimental Section

2.1. Materials

The following reagents were purchased from Sigma Aldrich: acetone, 2,2′-azobis(2-methylpropionitrile) (AIBN), chloroform, dichloromethane (DCM), ethylene glycol dimethacrylate (EGDMA), hexane, hexyl methacrylate (HM), methylene blue, oil red, petroleum ether, toluene, and 3-(trimethoxysilyl)propyl methacrylate (TMS). Aerosil R812S, a hydrophobic silica nanoparticle, was kindly supplied by Evonik. Gasoline and diesel were purchased from a local gas station. All chemicals were used without further purification. Deionized water (Millipore Milli-Q Academic water system) was used throughout this study. The stainless steel mesh screen (74 µm of pore opening) was purchased at a local hardware store, and a flat steel panel was purchased from Q-Lab. All the pictures were taken with a camera Sony Cyber-shot DSC-RX100.

2.2. Coating Preparation

The mesh screen was precleaned in acetone by sonication for 10 min, and dried with air. Two coatings were prepared: a methacrylate coating (hereafter named MC), and a methacrylate coating containing SiO_2 nanoparticles (hereafter named MC-1). MC was prepared by mixing HM, EGDMA, TMS and AIBN (1:0.05:0.05:0.01 w/w, respectively), and using toluene as solvent (1.5:1 w/w solvent/MC reagents). MC-1 was prepared by mixing HM, EDGMA, TMS and AIBN in the same proportions, adding 1% w/w of SiO_2 nanoparticles (SiO_2/MC reagents), and using toluene as solvent (1.5:1 w/w solvent/MC reagents + SiO_2). Finally, the mesh screen was then immersed in the coating, removed after 10 min, and reacted/cured in an oven at 100 °C for 20 min, as illustrated in **Figure 1**. For comparison purposes, a flat steel panel was precleaned and coated according to the same protocol of the mesh screen. For TGA analysis, the resin was prepared following the same procedure, except for not using the screen. The mixture was casted to obtain a thin film.

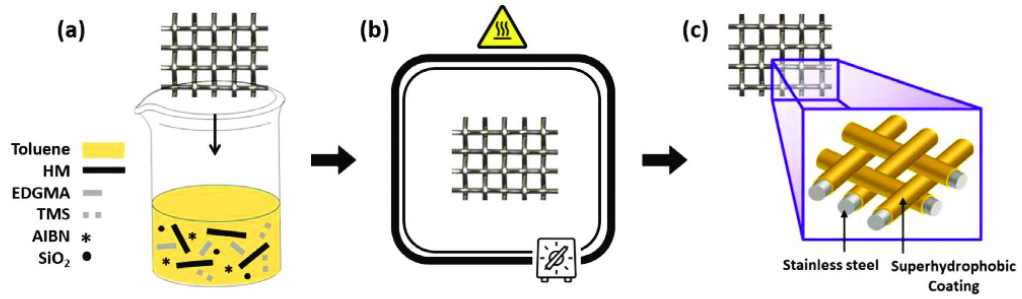

Figure 1. Representation of the a) MC-1 dip-coating, b) oven curing, and c) resulting superhydrophobic coated mesh screen.

2.3. Oil/Water Separation

A coated mesh screen (3 × 3 cm) was placed between two glasswares (2.0 cm of diameter) with open ends, and clamped together to provide stability and prevent any leakage. Without stirring, equal amounts of water (7 mL) and oil (7 mL) were added in a cylinder, and the content was poured onto the coated mesh screen, where the separation occurred solely based on gravity, without using any external pressure. The efficiency of separation (E) was determined gravimetrically according to Equation 1:

$$E = \left(\frac{m_1}{m_0}\right) \times 100 \quad (1)$$

where m_0 and m_1 are the mass of oil weighted before and after the separation, respectively.[11,13,15] The oil was collected in a glass vial placed underneath, and no water was observed in the collected oil. The experiments were carried out at 25 ± 2 °C, in triplicate, and the results represent the average ± standard deviation.

For recyclability evaluation of the MC-1 coating, tests were performed using water and petroleum ether mixture for twenty times, in the same conditions. Between cycles, the apparatus was cleaned with compressed air.

2.4. Characterization Methods

Rheological measurements were obtained on a TA Instruments ARES G2 rheometer using a 25 mm parallel plate geometry, at a frequency of 1 Hz, with a gap size of 1 mm, at 100 °C. For this analysis, the coating was casted on the plate and the reaction/cure was monitored over time. The static water contact angle of the coated substrates (mesh screen and flat steel panel) was measured by using a CAM 200 Optical Contact Angle Meter (KSV Instruments) at 25 ± 2 °C, considering 4–5 measurements throughout the surface, and the results represent the average ± standard deviation. The adhesion of MC-1 on the substrates was evaluated based on the ASTM standard test method D-3359,[30] where the coated substrate is scratched with a knife in a grid pattern, a tape is applied over the cross-cut area for 90 s, and the adhesion quality is classified visually after the tape is removed. SEM analysis was done with a Nova NanoLab 200 FIB/SEM at 15 kV. FTIR spectroscopy of the coated mesh screens was performed with a Cary 600 Series FTIR spectrometer in ATR mode (Agilent Technologies), with a nominal spectral resolution of 4 cm^{-1}, and average of 32 scans per run. TGA analyses of the resin were carried out using a thermogravimetric analyzer Q500 (TA Instruments, USA). Nonisothermal TGA was performed from 25 to 650 °C at different heating rates: 5, 10, 20 and 40°C min^{-1}. Isothermal TGA was performed at 100, 125, 150, and 175 °C for 120 min. All TGA experiments were carried out under N_2.

3. Results

3.1. Chemorheology of the Curing Reaction

Chemorheology is the study of the flow properties of the reactive polymer system, and it has been widely used to investigate the cure behavior of different polymeric materials.[31–34] From the practical standpoint, coatings have to flow during their application. In other words, the viscosity of the coating formulation has to be low enough in order to provide a homogenous distribution of the coating on a substrate, what can dramatically impact the final properties of the coated surfaces.[35] For thermosetting coatings, the viscosity plays an important role during the crosslinking reaction, and the understanding of how the viscosity evolves over time is of utmost relevance for the design and optimization of a cure process.[36]

Figure 2 shows the evolution of the complex viscosity ($|\eta^*|$) over time for MC-1, at 100 °C. Three different stages of reaction kinetics can be easily identified on the curve: i) an induction period, ii) polymerization, and iii) termination, where the viscosity reaches a plateau. During the induction period (i), there is no significant change in viscosity due to the competing effects of heat transfer, which tend to decrease the viscosity due to the temperature equilibration (from room temperature to 100 °C), and the polymerization reaction, which tends to increase the viscosity as the reaction progresses. During the polymerization (ii), there is a pronounced increase in viscosity as higher macromolecular structures are formed. At a later stage of the polymerization (≈350 s), the viscosity increase starts to be suppressed due to a decrease of reacting species in the high viscous media, until the reaction is considered terminated by reaching a plateau (iii).[32]

Chemorheology results indicated that the coating is completely cured at 20 min at 100 °C, what represents a substantial reduction in the production time when compared to other superhydrophobic coatings.[11,14,16] These conditions of time and temperature were used to produce the coating on the mesh screen.

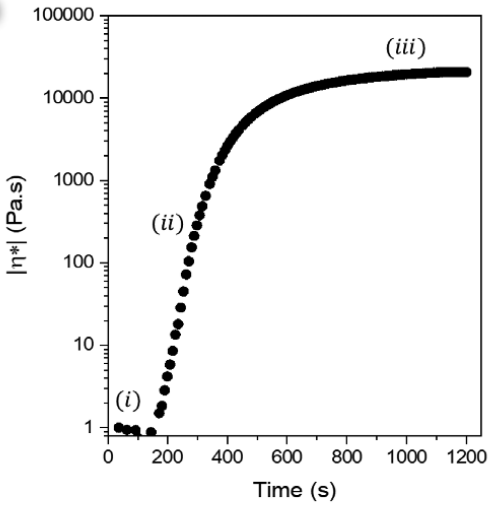

Figure 2. Evolution of the complex viscosity as a function of time for MC-1, at 100 °C.

3.2. Characterization of the Superhydrophobic Coating

In order to assess the wetting behavior of the coatings, the water contact angle (CA) was measured on the coated mesh screen (**Figure 3**a), as well as the sliding angle (SA). The MC coating exhibited a hydrophobic surface with a CA of 121 ± 2° (Figure 3b), which is associated with the hydrophobic nature of the alkyl tail of the HM, and the network structure formed with the silane (TMS) and crosslinker molecules (EDGMA). Upon incorporation of SiO_2 nanoparticles, the coating MC-1 showed a CA of 162 ± 2° (Figure 3c) and a SA of 4 ± 1°, besides exhibiting a rougher surface with nanometrical structures thoroughly covering the substrate (Figure 3e), if compared with the MC coated surface (Figure 3d). For comparison purposes, a flat substrate was coated with MC-1 under the same conditions, and it exhibited a CA of 157 ± 2° and a SA of 5 ± 1°. According to the Cassie-Baxter model, rough surfaces can trap air in their cavities, resulting in a higher water CA if compared to smooth surfaces.[37] Therefore, the roughness enhancement afforded by the incorporation of SiO_2 nanoparticles effectively led to a superhydrophobic behavior in MC-1 for both substrates (mesh screen and flat panel). The CA of the coated flat panel was lower than the CA of the coated mesh screen, probably due to the structural waviness of the later, which favors the water repellency. However, both CA values were higher than 150° and both SA values were lower than 10°, demonstrating that the coating MC-1 exhibited a superhydrophobic character for both substrates.

Indeed, superhydrophobicity is often achieved by the conjunct effort of the chemical structure of the coating (with hydrophobic nature) and its morphological tuning in order to meet the Cassie-Baxter state. Caldona and co-workers designed a coating based on a rubber-modified polybenzoxazine, achieving a CA of 101 ± 1°, and they incorporated hydrophobic fumed silica nanoparticles up to 50 wt%, increasingly enhancing the CA up to 158 ± 1°.[12] Sheng and co-workers obtained amino-silicone oil/polyacrylonitrile membranes with a CA of 145°, and decorated them with up to 0.4 wt% of hydrophobic silica nanoparticles, raising the CA to 151°.[29] Similarly, Li et al. fabricated a coating based on candle soot, followed by the deposition of hydrophobic silica nanoparticles in order to reach superhydrophobicity, with a CA of 160 ± 1°.[15]

To corroborate with the CA values and morphological observations, FTIR was used to confirm the effective formation of the superhydrophobic coating. Figure 3f shows the FTIR spectrum for the MC-1 coating, exhibiting an intense peak at 1147 cm^{-1} associated with the C—O—C stretching, and another one at 1727 cm^{-1} corresponding to the ester C=O stretching. The peaks at 2852 and 2920 cm^{-1} were associated with the CH_3 symmetric and asymmetric stretchings, respectively, whereas the peak at 1465 cm^{-1} is related to the C—H bending of the methylene groups. The absence of peaks at 1650 and 3090 cm^{-1} respectively associated with C=C and =C—H stretching bands, demonstrated that the crosslinking reaction was completed.[38]

The adhesion of the coating MC-1 on steel substrates (mesh screen and flat panel) was evaluated by the "scratch test," as described by the ASTM standard test method D-3359[30] (**Table 1**). Regardless of the substrate, the edges of the cuts looked smooth, and none of the squares of the lattice peeled off after removing the tape. Furthermore, the wettability of the coated substrates after the scratch test was evaluated, specifically within the cross-cut area. Both coated substrates retained their superhydrophobicity, exhibiting CA (and SA) values of 156 ± 2° (6 ± 1°) and 156 ± 1° (6 ± 1°) for the flat panel and mesh screen, respectively. Therefore, the coating MC-1 exhibited an excellent adhesion property on the refereed substrates, and it kept its prominent water repellency even after the scratch test. This result also demonstrates that the nanoparticles were well stabilized in the resin during the curing reaction, since the asperities of the coating surface were not removed by the tape. The stability and integrity of the coating are associated with the strong and extensive interactions between the polymer network and the substrate, enhanced by the Si—O—R linkages from the silane used in the coating formulation. Other polymeric coatings also reported the use of silanes to improve their adhesion properties.[9,11,13,16]

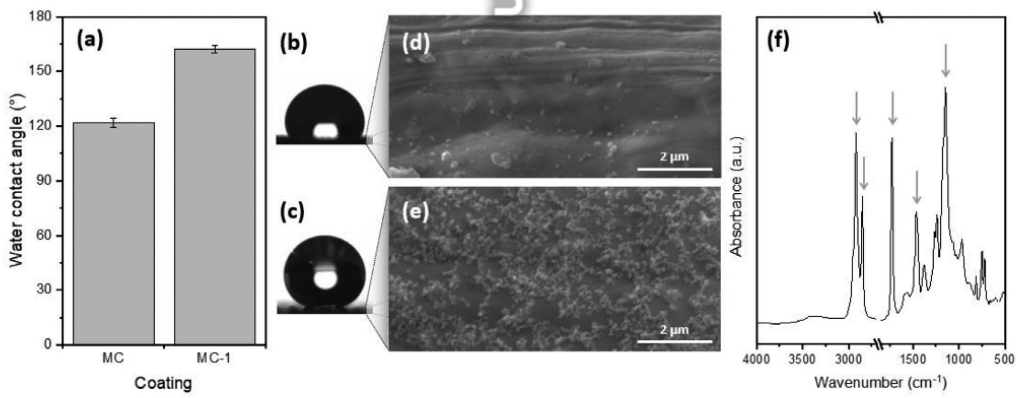

Figure 3. a) Water CA values for the MC and MC-1 coated mesh screen, and CA images for b) MC and c) MC-1. SEM images for the d) MC and e) MC-1 coatings. f) FTIR spectrum of the MC-1 coating.

Table 1. Evaluation of the MC-1 coating adhesion on different steel substrates according to the ASTM standard test method D-3359.[30].

Substrate	Visual inspection after the test	ASTM D-3359	
		Area removed [%]	Classification
Mesh screen	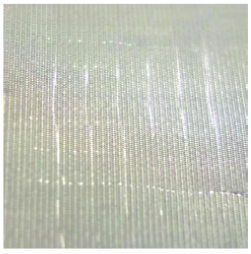	0	5B
Flat panel	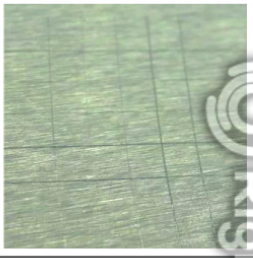	0	5B

The efficiency of oil/water separation and the thermal stability study were carried out only using the coating MC-1, since it exhibited the superhydrophobic character.

3.3. Efficiency of Superhydrophobic Coating in the Oil/Water Separation

In order to assess the viability of the MC-1 coating for oil/water separation, both water and oil were separately poured on the coated mesh screen. To aid visualization, water was dyed blue using methylene blue, while petroleum ether was dyed red using oil red. As shown in **Figure 4**a, when only water was introduced on the top of the coated screen, it accumulated on the upper part, and no trace of water was found in the vial placed underneath over several hours. On the other hand, when only petroleum ether was introduced (Figure 4b), it instantaneously passed through the coated mesh screen, and it was collected in the vial. The same occurred when different types of oils (gasoline, diesel, hexane, toluene, chloroform, and DCM) were tested individually. These observations demonstrate that the superhydrophobic coating is also superoleophilic. This behavior can be explained in terms of the inherent oleophilic nature of MC-1, and the fact that its improved surface roughness enhances the wettability to oils as predicted by the Wenzel equation.[39]

Therefore, the superhydrophobic/superoleophilic coating MC-1 can be used for oil/water separation, since it can selectively prevent the water passage, but let the oil flow through the pores of the coated screen (as illustrated in **Figure 5**a).[12–14]

A variety of water and oil mixtures were prepared, and the gravity-driven oil/water separation experiment was carried out using the MC-1 coated screen. As an example, Figure 5b shows the experimental setup for the separation of water (dyed blue) and petroleum ether (dyed red). When the liquids were poured onto the coated mesh screen, only the oil selectively passed through it, being collected in the vial, while the water stayed in the upper part. The separation efficiency of the MC-1 coating for different oil/water mixtures is shown in Figure 5c. MC-1 exhibited an outstanding separation efficiency for seven different types of oil widely used in different applications, exhibiting values as high as 99% for diesel, petroleum ether and hexane. **Table 2** shows a comparison of the separation efficiency of different oil/water mixtures by superhydrophobic coatings in the literature, using similar procedures. For simplification, we proposed a classification of the separation efficiency (E) as follows: "A" for $E \geq 95\%$, "B" for $90\% \leq E < 95\%$, and "C" for $E < 90\%$. The superhydrophobic/superoleophilic coating MC-1 stood out for exhibiting a quality "A" efficiency of separation for different types of oils, making it a very strong candidate for efficiently cleaning up oil spills from different sources and activities, as well as being suitable for improving industrial separation processes. As an example, Cao and co-workers obtained a superhydrophobic coating based on polyurethane/SiO_2, exhibiting quality "A" efficiency of separation for water/toluene and water/kerosene mixtures. However, it exhibited quality "B" for petroleum ether, hexane and tetrachloromethane mixtures with water.[9] Note that many of the reported works in Table 2 took advantage of incorporating SiO_2 nanoparticles for enhancing the surface

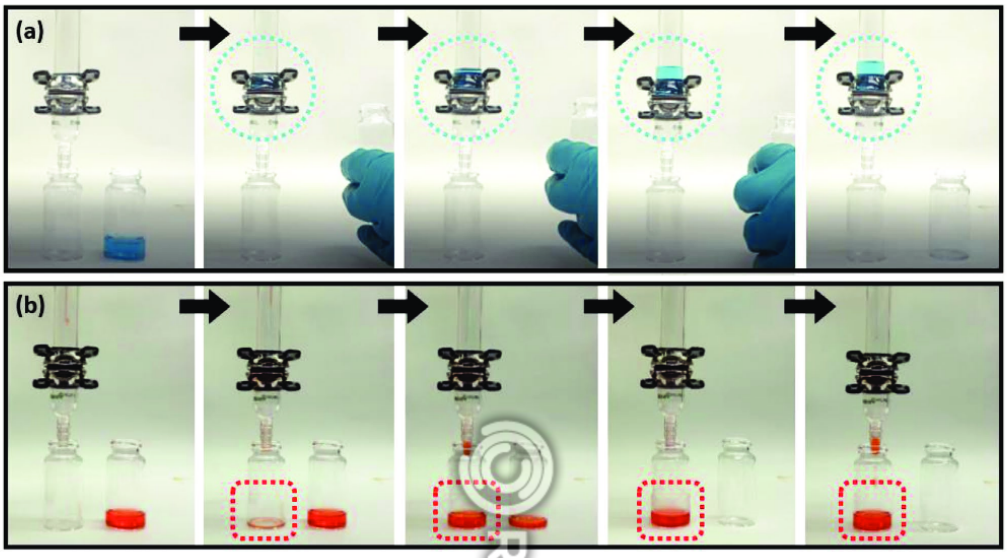

Figure 4. Photographs of the experimental setup to demonstrate the superhydrophobic and superoleophilic character of MC-1, where a) water (dyed blue) accumulated on the top of the coated screen, and b) petroleum ether (dyed red) immediately passed through it, being collected in the bottom. The black arrows indicate the progress of time.

roughness, and therefore achieving the Cassie-Baxter state, as discussed before.[9,10,12,13,15,16]

Finally, the assessment of the recyclability of the MC-1 coating for water/petroleum ether is shown in Figure 5d. The superhydrophobic/superoleophilic coating maintained the separation efficiency approximately constant, exhibiting a quality "A" efficiency even after 20 cycles, demonstrating its durability. Kang and co-workers obtained a superhydrophobic coating based on nanostructured titania, and they reported a quality "A" efficiency over 10 cycles for hexane and water mixtures.[28]

3.4. Thermal Analysis

Despite the vast number of papers describing the applications of superhydrophobic coatings, very few discuss their thermal degradation and thermal properties.[40,41] Herein we present a discussion on the isothermal and nonisothermal degradation, and an evaluation of the surface wettability changes with temperature and time, in correlation with structural changes.

3.4.1. Isothermal and Nonisothermal Degradation

Isothermal TGA is a convenient tool to evaluate the thermal stability of thermosets.[5,42,43] **Figure 6**a shows the Isothermal TGA for the MC-1 superhydrophobic/superoleophilic coating at different temperatures over 120 min. At 100 °C, no thermal degradation was observed. This observation further validated the curing condition found by chemorheology (Section 3.1). As the temperature progressively increased to 150 °C, the slope of the weight loss became slightly more noticeable, until reaching 175 °C where the thermal degradation was quicker at earlier times. This observations demonstrate that the coating MC-1 can be used in applications that require high temperature.

Figure 6b shows the nonisothermal TGA for the MC-1 coating at different heating rates, exhibiting a slow multistep thermal degradation in the range of 120–550 °C. When the heating rate was increased, the weight loss rate was slightly decreased due to heat transfer limitations, as observed in other polymeric materials.[42,44] In thermal analysis, $T_{5\%}$ and $T_{10\%}$ are defined as the temperature at which the weight loss is 5% and 10%, respectively. For MC-1, both $T_{5\%}$ and $T_{10\%}$ progressively increased as the heating rate increased from 5 to 40 °C min^{-1} (**Table 3**), illustrating the thermal lag. A polyurethane-based coating developed for concrete structures exhibited a $T_{5\%}$ of 134.3 °C at 20 °C min^{-1}, which is significantly lower than the result obtained for the superhydrophobic/superoleophilic coating MC-1 in this study.[45] The thermal lag effect was further evidenced by the DTG curves (Figure 6c), as the peak temperatures shifted to higher temperatures when the heating rate increased. Furthermore, at 5 °C min^{-1}, the DTG exhibited five peaks (201.2, 306.9, 358.8, 405.0, and 475.3 °C). However, as the heating rate increased, some of the thermal events merged, giving rise to only two broader peaks.

Bertini et al. studied a series of poly-*n*-alkyl acrylates (PAA) and poly-*n*-alkyl methacrylates (PMA) of different carbon length using gas chromatography/mass spectrometry. The general mechanism of PAA thermal degradation included random main-chain scission and side-chain reactions leading to the

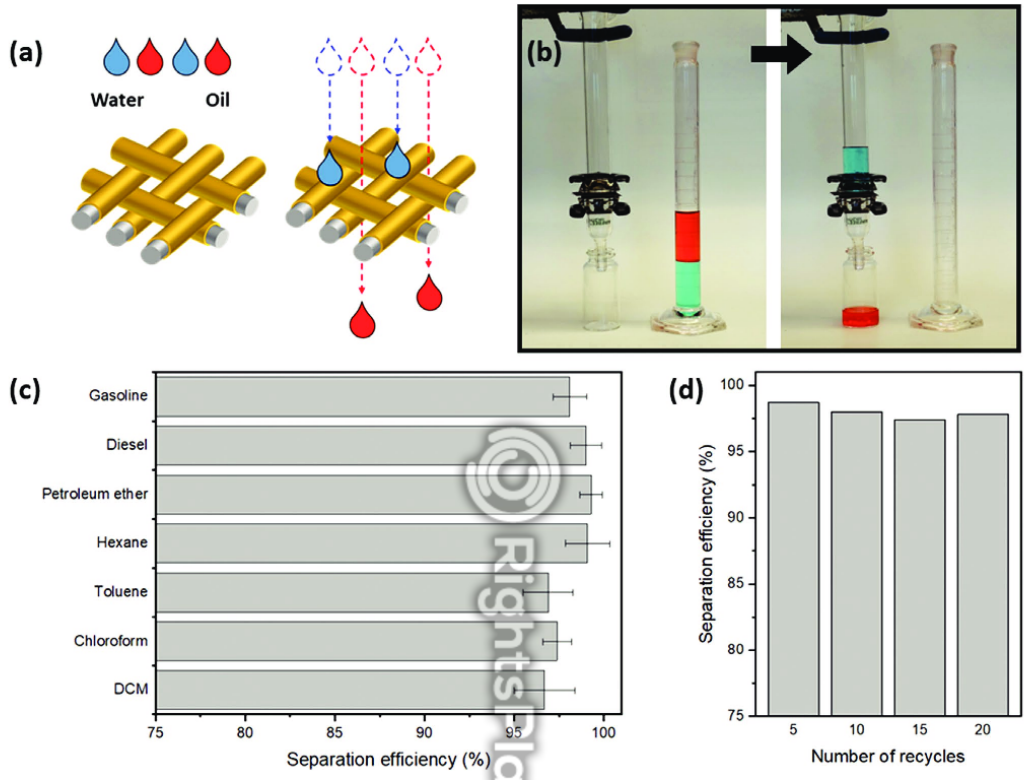

Figure 5. a) Representation of the superhydrophobic/superoleophilic behavior, where water droplets stay on top of the coated screen, and the oil droplets pass through the pores. b) Experimental setup for the separation of water (dyed blue) and petroleum ether (dyed red), where only the oil selectively permeated the coated screen. c) Separation efficiency of different oil/water (50:50) mixtures by the MC-1 coated screen. d) Recyclability of the MC-1 coating for the water and petroleum ether mixture.

Table 2. Comparison of the separation efficiency (*E*) of different oil/water mixtures by coated mesh screens.

Superhydrophobic Coating	Efficiency[a] of oil/water separation								Reference
	Gasoline	Diesel	Petroleum ether	Kerosene	Hexane	Toluene	Chloroform	Dichloromethane	
Methacrylate-based/SiO_2	A	A	A	–	A	A	A	A	This study
Candle soot/SiO_2	–	–	A	A	A[b]	A	A	–	[15]
Epoxy resin/SiO_2	–	A	–	A	B	B	A	–	[13]
Polyurethane/SiO_2			B	A	B	A		B[c]	[9]
Polydimethylsiloxane/SiO_2/TiO_2	–	–	–	–	C	A	–	A	[16]
Silicone-acrylic copolymer	–	–	–	–	–	–	–	A	[11]
Polystyrene/SiO_2	–	D	–	–	–	–	–	–	[10]
Polybenzoxazyne/SiO_2	–	–	–	–	–	–	–	D	[12]
Electrodeposited polythiophene	–	–	–	–	–	–	–	D	[4]

[a]"A" was used when $E \geq 95\%$, "B" when $90\% \leq E < 95\%$, "C" when $E < 90\%$, and "D" was used when *E* was not reported; [b]The authors used heptane; [c]The authors used tetrachloromethane.

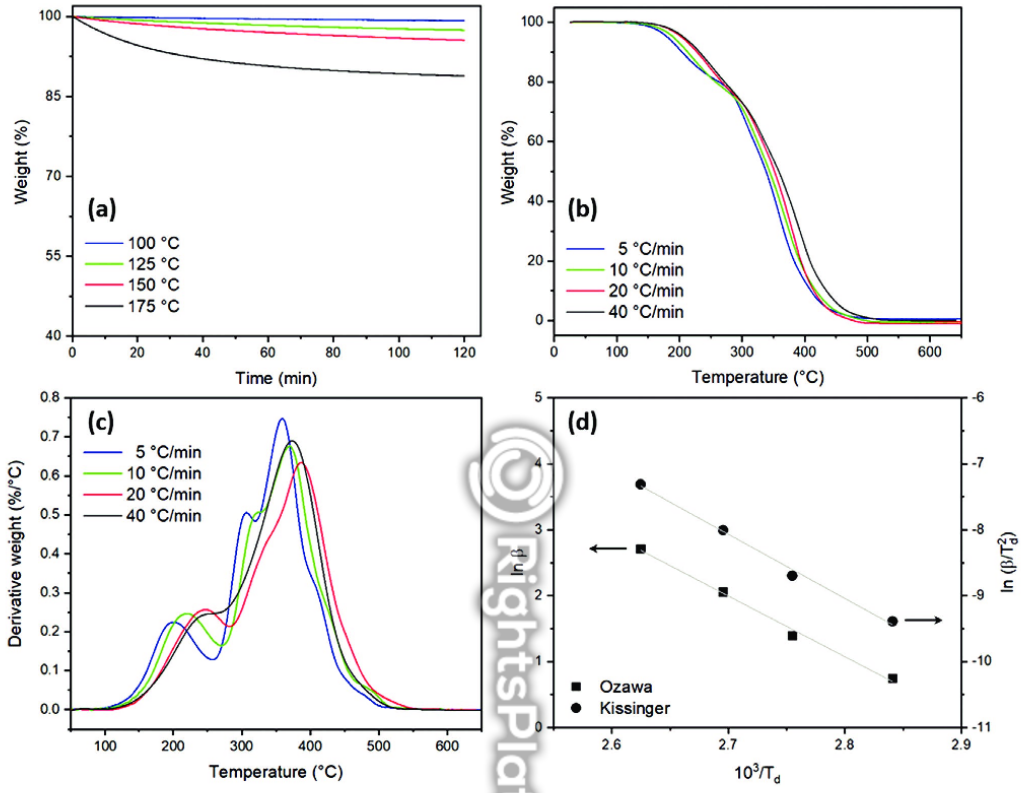

Figure 6. a) Isothermal TGA for the MC-1 superhydrophobic/superoleophilic coating at different temperatures over 120 min. b) Nonisothermal TGA and c) TGA first derivative at different heating rates for the MC-1 coating. d) Plots of the Ozawa and Kissing equations. All TGA tests were performed under N_2.

formation of the monomer, dimer, trimer, diester, alcohol, aldehyde, acetate, olefins, and methacrylate. On the other hand, the mechanism of PMA thermal degradation included hemolysis of the chain, and possibly side group ester decomposition favoring the formation of the monomer, but also obtaining olefin and methacrylic acid.[46] Considering the complex structure of the superhydrophobic/superoleophilic coating in the present study, it is very challenging to detail the chemical pathways of the thermal degradation processes, since it may encompass several heterogeneous reactions taking place in parallel and/or in sequence. However, the assessment of the thermal stability of coatings is of high relevance for the whole industrial chain, from fabrication to end-user application.

Besides discussing the isothermal and nonisothermal degradation, we want to provide physicochemical parameters from thermokinetic models, such as the activation energy of thermal degradation. This discussion not only highlights the importance of the structure-property relationship in polymer science,

Table 3. Thermal properties of MC-1.

TGA parameters			Thermokinetics		
Heating rate [°C min^{-1}]	$T_{5\%}$ [°C]	$T_{10\%}$ [°C]	Method	Ea [kJ mol^{-1}]	R^2
5	180.8	204.1	Kissinger	113.5	0.9962
10	190.4	213.1			
20	203.7	227.9	Ozawa	114.0	0.9966
40	206.7	232.0			

but also provides complementary quantitative information that is relevant for materials being considered for high temperature applications.

The Kissinger model (Equation 2),[47] initially developed for differential scanning calorimetry (DSC), was later demonstrated to be applicable to TGA.[42,48] In addition, the Ozawa model (Equation 3) has been widely employed for kinetic calculations based on TGA data.[49] Both models rely on the fact that the plot of a function of the heating rate versus the reciprocal absolute temperature gives a straight line, and the activation energy can be calculated from its slope. Hence, these models require a minimum of three different heating rates in order to calculate the activation energy. Some works in literature were based on three heating rates,[50,51] however, we have used four heating rates in this study for accuracy purposes.

$$\ln\left(\frac{\beta}{T_d^2}\right) = \ln\left(\frac{AR}{E_a}\right) - \frac{E_a}{RT_d} \quad (2)$$

$$\ln\beta = -1.052\frac{E_a}{RT_d} + C \quad (3)$$

where β is the heating rate, A is the frequency factor, R is the gas constant, T_d is the on-set temperature of degradation, E_a is the activation energy of thermal degradation, and C is a constant.

Figure 6d shows the plot of $\ln(\beta/T_d^2)$ as well as $\ln(\beta)$ as a function of $1/T_d$ according to the models of Kissinger and Ozawa, respectively. As shown in the Figure, straight lines were obtained for both models, exhibiting very high correlation coefficient (Table 3). Finally, the E_a was calculated as 113.5 and 114.0 kJ mol^{-1} for the Kissinger and Ozawa models, respectively.

3.4.2. Thermal Ageing of MC-1: CA and Structural Changes

Considering that 175 °C caused the most prominent effect on the isothermal TGA (Figure 6a), the thermal ageing was performed at the temperature of 150 °C. **Figure 7**a shows the effect of the thermal ageing on the CA of the MC-1 coated screen. At 30 min, the surface lost its superhydrophobic character, exhibiting a CA of 143 ± 3°. The CA exhibited a smooth decrease up to 129 ± 1° at 120 min of thermal ageing. This is probably associated with the thermal degradation of the coating, which changed its chemical structure and reduced the water repellent ability.

FTIR has been used to demonstrate structural changes of polymeric materials during thermal and photo ageing by identifying ageing-sensitive bands on the spectra collected over time.[52] The peak at 1147 cm^{-1} (C—O—C stretching) on Figure 7b remained almost unchanged with the ageing conditions, and therefore it was chosen as a reference for normalization purposes.[53] Examination of the FTIR spectra of thermal aged MC-1 reveals the emergence of the peak at 1727 cm^{-1} (carbonyl stretching), possibly related to the generation of thermal oxidation products. On the other hand, it was observed a decrease on the peak at 1240 cm^{-1} (methyl rocking), which is probably due to the alkyl tail scission of the alkyl methacrylate.[54]

Interestingly, the normalized absorbance ratios A_{1727}/A_{1147} and A_{1240}/A_{1147} exhibited an upward (Figure 7c) and downward (Figure 7d) linear correlation with time, respectively. This suggests that MC-1 has a very short induction time, if any. The linear equations found were: $A_{1727}/A_{1147} = 0.0021t + 0.7648$ ($R^2 = 0.995$) and $A_{1240}/A_{1147} = -0.0018t + 0.4862$ ($R^2 = 0.988$). A recent report by Morsch and co-workers discussed the thermal oxidative degradation of an epoxy-amine resin, where peaks at 1738 and 1658 cm^{-1} emerged over time during thermal ageing at 60 °C, and exhibited a linear trend.[55]

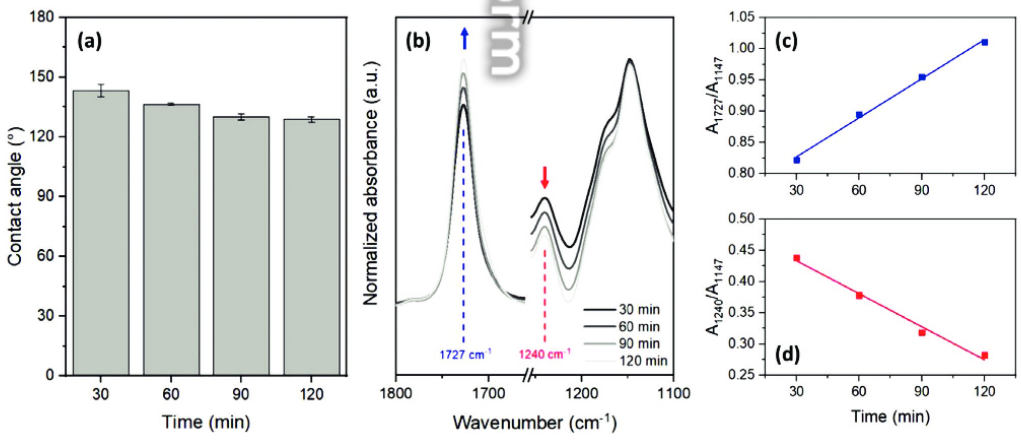

Figure 7. Thermal ageing: a) water CA values and b) FTIR spectra for the MC-1 coated mesh screen for different ageing times at 150 °C (the arrows indicate the increasing or decreasing spectral changes observed with increasing ageing times). Plots of the c) 1727 cm^{-1} and d) 1240 cm^{-1} absorbances normalized to 1147 cm^{-1}.

The CA changes evidenced the impact of the thermal ageing on the wettability of the coating, and FTIR provided time-sensitive information regarding the structural changes.

4. Conclusions

We have demonstrated a rapid and efficient way to obtain a superhydrophobic/superoleophilic methacrylate-based, fluorine-free coating by a simple two-step procedure: dip-coating and oven curing for 20 min. The coatings with (MC-1) and without (MC) SiO_2 nanoparticles exhibited a contact angle of 162 ± 2° and 121 ± 2° for the mesh screen, respectively. The superhydrophobic character of MC-1 for a flat substrate was also confirmed by contact angle (157 ± 2°) and sliding angle (5 ± 1°). The MC-1 coated mesh screen exhibited excellent adhesion properties, and an outstanding performance of oil/water separation when tested with seven different oils of wide industrial interest: petroleum ether, gasoline, diesel, hexane, toluene, chloroform and dichloromethane (96–99%). The superhydrophobic coating maintained its high separation efficiency of water/petroleum ether even being recycled for 20 times. These observations encourage further investigation of more specific applications, such as breaking water-in-oil emulsions. Isothermal and non-isothermal TGA highlighted the superior thermal stability of the MC-1 coating, which was well described by the Kissinger and Ozawa methods, and the activation energy of thermal degradation was calculated as 113.5 and 114 kJ mol^{-1}, respectively. During thermal ageing at 150 °C, the contact angle of MC-1 coated mesh screen decreased up to 129 ± 1° over time, and FTIR analysis showed structural changes possibly related to the generation of thermal oxidation products.

Acknowledgements

This study was supported in part by the Coordenação de Aperfeiçoamento de Pessoal de Nível Superior – Brasil (CAPES) – Finance Code 001. Elizabete Lucas thanks FAPERJ (E-26/202.877/2017) and CNPq (307193/2016-0).

Conflict of Interest

The authors declare no conflict of interest.

Keywords

oil/water separation, superhydrophobic materials, superoleophilic materials, thermal degradation, thermosetting methacrylate

Received: June 25, 2020
Revised: August 24, 2020
Published online: September 23, 2020

[1] Organization of Petroleum Exporting Countries, *Lead. Edge* **2017**, https://www.opec.org/opec_web/static_files_project/media/downloads/publications/ASB2017_13062017.pdf (accessed: August 2019).
[2] U.S. Energy Information Administration, https://www.eia.gov/tools/faqs/faq.php?id=23&t=10 (accessed: June 2020).
[3] E. F. Lucas, C. R. E. Mansur, L. Spinelli, Y. G. C. Queirós, *Pure Appl. Chem.* **2009**, *81*, 473.
[4] A. C. Leon, R. E. S. Imperial, Q. Chen, R. C. Advincula, *Macromol. Mater. Eng.* **2019**, *304*, 1800722.
[5] T. K. L. Nguyen, S. Livi, B. G. Soares, G. M. O. Barra, J.-F. Gérard, J. Duchet-Rumeau, *ACS Sustainable Chem. Eng.* **2017**, *5*, 8429.
[6] A. Acosta-González, S. M. Martirani-von Abercron, R. Rosselló-Móra, R. M. Wittich, S. Marqués, *Environ. Sci. Pollut. Res.* **2015**, *22*, 15200.
[7] M. Schrope, *Nature* **2011**, *472*, 152.
[8] The Guardian, https://www.theguardian.com/business/2018/jan/16/bps-deepwater-horizon-bill-tops-65bn (accessed: January 2020).
[9] M. Cao, X. Luo, H. Ren, J. Feng, *J. Colloid Interface Sci.* **2018**, *512*, 567.
[10] B. Li, X. Liu, X. Zhang, W. Chai, *Eur. Polym. J.* **2015**, *73*, 374.
[11] H. Ye, L. Zhu, W. Li, H. Liu, H. Chen, *J. Mater. Chem. A* **2017**, *5*, 9882.
[12] E. B. Caldona, A. C. C. De Leon, P. G. Thomas, D. F. Naylor, III, B. B. Pajarito, R. C. Advincula, *Ind. Eng. Chem. Res.* **2017**, *56*, 1485.
[13] Z. H. Zhang, *et al.*, *Sci. Rep.* **2018**, *8*, 1.
[14] H. Y. Lai, A. de Leon, K. Pangilinan, R. Advincula, *Prog. Org. Coat.* **2018**, *115*, 122.
[15] J. Li, R. Kang, X. Tang, H. She, Y. Yanga, F. Zha, *Nanoscale* **2016**, *8*, 7638.
[16] F. L. Heale, M. Einhorn, K. Page, I. P. Parkin, C. J. Carmalt, *RSC Adv.* **2019**, *9*, 20332.
[17] B. Samuel, H. Zhao, K. Y. Law, *J. Phys. Chem. C* **2011**, *115*, 14852.
[18] D. Soto, A. Ugur, T. A. Farnham, K. K. Gleason, K. K. Varanasi, *Adv. Funct. Mater.* **2018**, *28*, 1707355.
[19] H. Wang, H. Zhou, A. Gestos, J. Fang, H. Niu, J. Ding, T. Lin, *Soft Matter* **2013**, *9*, 277.
[20] U.S. Environmental Protection Agency, https://www.epa.gov/pfas (accessed: June 2020).
[21] C. Lau, J. L. Butenhoff, J. M. Rogers, *Toxicol. Appl. Pharmacol.* **2004**, *198*, 231.
[22] A. De Leon, R. C. Advincula, *ACS Appl. Mater. Interfaces* **2014**, *6*, 22666.
[23] B. D. B. Tiu, H. N. Nguyen, D. F. Rodrigues, R. C. Advincula, *Macromol. Symp.* **2017**, *374*, 1600138.
[24] R. B. Pernites, R. R. Ponnapati, R. C. Advincula, *Adv. Mater.* **2011**, *23*, 3207.
[25] A. C. C. De Leon, R. B. Pernites, R. C. Advincula, *ACS Appl. Mater. Interfaces* **2012**, *4*, 3169.
[26] R. B. Pernites, C. M. Santos, M. Maldonado, R. R. Ponnapati, D. F. Rodrigues, R. C. Advincula, *Chem. Mater.* **2012**, *24*, 870.
[27] E. L. Foster, A. C. C. De Leon, J. Mangadlao, R. Advincula, *J. Mater. Chem.* **2012**, *22*, 11025.
[28] H. Kang, H. Kang, Z. Cheng, H. Lai, H. Ma, Y. Liu, X. Mai, Y. Wang, Q. Shao, L. Xiang, X. Guo, Z. Guo, *Sep. Purif. Technol.* **2018**, *201*, 193.
[29] J. Sheng, Y. Xu, J. Yu, B. Ding, *ACS Appl. Mater. Interfaces* **2017**, *9*, 15139.
[30] ASTM, *Annu. B. ASTM Stand.* **2009**, 1, https://doi.org/10.1520/D3359-17 (accessed: August 2020).
[31] A. Patel, A. Maiorana, L. Yue, R. A. Gross, I. Manas-Zloczower, *Macromolecules* **2016**, *49*, 5315.
[32] V. Solouki Bonab, I. Manas-Zloczower, *Polymer* **2016**, *99*, 513.
[33] R. Foudazi, P. Gokun, D. L. Feke, S. J. Rowan, I. Manas-zloczower, *Macromolecules* **2013**, *46*, 5393.
[34] S. A. Madbouly, Y. Xia, M. R. Kessler, *Macromolecules* **2012**, *45*, 7729.
[35] R. R. Eley, *J. Coat. Technol.* **1984**, *56*, 49.
[36] J. D. Menczel, R. B. Prime, *Thermal Analysis of Polymers: Fundamentals and Applications*, Wiley, New York **2008**.

